Available online at www.sciencedirect.com
SCIENCE DIRECT®
International Journal of Thermal Sciences 44 (2005) 289–301
International Journal of Thermal Sciences
www.elsevier.com/locate/ijts

Influence of CrN coating in wood machining from heat flux estimation in the tool

Andrzej Kusiak [a,*], Jean-Luc Battaglia [a], Rémy Marchal [b]

[a] *TREFLE – site ENSAM, UMR 8508, esplanade des arts et métiers, 33405 Talence cedex, France*
[b] *LABOMAP, EA 3633, École nationale supérieure d'arts et métiers, rue porte de Paris, 71250 Cluny, France*

Received 28 January 2004; received in revised form 8 July 2004; accepted 18 August 2004
Available online 18 November 2004

Abstract

The influence of CrN coating on the thermal phenomena during wood composite (MDF—medium density fiberboard) peeling is investigated. The heat flux in the knife is used as the thermal indicator of the coating impact. The heat flux estimation is obtained through the resolution of the inverse heat conduction problem in the tool. The difficulty encountered in this problem comes from the great uncertainty in the sensors location and on the nonlocal measurement. The noninteger system identification method is used in order to obtain an accurate heat transfer model in the tool that rely the spatial average heat flux on the cutting edge to the temperature of the sensors embedded in the tool along the time. This average heat flux is then estimated during machining using the classical constant function specification method. The spatial variation of the heat flux on the cutting edge is reached using a finite element approach and its magnitude is adjusted with respect to the value of the estimated average heat flux.

Keywords: Heat flux; Tool coating; Non-integer differentiation; Inverse heat conduction problem; Wood machining

1. Introduction

The machining operation is one of the most important in transformation of raw materials to final products. During cutting process a tool in wedge form removes a part of machined material called chip. Numerous complex intensive interactions occur in the cutting zone. These interactions result in different products like vibrations, noise and acoustic emissions, friction, plastic and elastic deformations, chemical reactions and heat generation. Finally, their effects are machined surface quality on the workpiece part and tool wear on the processing system side. These phenomena take place both in continuous and interrupted cutting; they are also present during machining of relatively low specific gravity materials like wood or wood composites. Composite wood products machining increase the significance of phenomena occurring in the neighbourhood of tool. It is well known that machining wood based products causes wearing out of tool faster than when solid wood cutting. It comes from their higher mineral particle rate and adhesive contents. Because of this, carbide cutting tools have been introduced into secondary transformation of wood. The best cutting qualities and wear resistance are obtained with polycrystalline diamond (PCD) tools, nevertheless very expensive. Carbide inserts are cheaper, but do not provide as good performance as PCD inserts. Present directions in tooling research are scoped on tool surface modifications in order to improve tool life and performance and do not increase drastically the costs [1].

The present study concerns the machining configuration represented in Fig. 1 called the peeling process. It consists in removing material from a natural or composite wood disk using a steel knife. In this process, the wood chip named veneer is the final product used for different applications: plywood, LVL (laminated veneer lumber), furniture coatings, packaging etc. The cutting parameters are the cutting

* Corresponding author. Tel.: +33 556 845 426, fax: +33 556 845 401.
E-mail address: andrzej.kusiak@bordeaux.ensam.fr (A. Kusiak).

1290-0729/$ – see front matter
doi:10.1016/j.ijthermalsci.2004.08.006

Nomenclature

$\mathbf{A}$	state matrix (N × N)	
$\mathbf{B}$	control matrix	
$\mathbf{C}$	observation matrix	
$\mathbf{C}_p$	matrix of heat capacity (N × N)	
$e(t)$	measurement error at time t	K
$\mathbf{E}_K$	residue vector	
F_c	cutting force	N
$h(t)$	impulse response at time t	
$\mathbf{H}_K$	regression matrix	
K	number of measurements	
L	distance	m
l	tool chip contact length	m
l'	tool workpiece contact length	m
n_i	reel integration/differentiation order	
N	order of noninteger model reduction	
N	dimension of the complete model	
r	number of future time steps	
t	time	s
$T(t)$	temperature at time t	K
$\mathbf{U}(t)$	input vector	
$\widehat{\mathbf{U}}(t)$	estimated input vector	
V_a	cutting speed	$\mathrm{m{\cdot}s^{-1}}$
V_f	feed speed	$\mathrm{m{\cdot}min^{-1}}$
X_c	horizontal component of F_c	N
Y_c	vertical component of F_c	N
$Y(t)$	temperature measurement at time t	K
$\mathbf{Y}_K$	temperature measurements vector	
V	voltage	V

Greek symbols

α	thermal diffusivity	$\mathrm{m^2{\cdot}s^{-1}}$
α_i, β_i	noninteger model parameters	
α	clearance angle	°
β	tool angle	°
γ	rake angle	°
Δt	sampling period	s
$\delta(t)$	Dirac function	
$\varepsilon(t)$	residue at time t	
$\phi(t)$	heat flux	W
ϕ_c	heat flux in the chip	W
ϕ_t	heat flux in the tool	W
ϕ_w	heat flux in the workpiece	W
$\hat{\phi}(t)$	estimated heat flux	W
σ_Y	standard deviation on Y	
$\boldsymbol{\theta}$	parameters vector of noninteger model	
$\hat{\boldsymbol{\theta}}$	estimated parameters vector of noninteger model	

Operators

$\mathrm{D}^{\nu} f(t)$	fractional derivative ν order of $f(t)$
$\mathrm{I}^{\nu} f(t)$	fractional integral ν order of $f(t)$
Γ	gamma function

Subscripts

M	measurement location
i, j, l	iteration index

velocity V_a and the feed rate V_f. The micro lathe used in this application is designed in order to impose a constant value for V_a by adjusting the angular velocity of the disk according to its diameter [2]. The cutting force orthogonal components X_c and Y_c on the tool are measured with embedded piezoelectric sensors. These measurements lead to determine the mechanical power consumed during peeling. The process can be viewed, without making any geometrical approximations as an orthogonal cutting representation. MDF (Medium Density Fiberboard) disks are used as the workpieces in the studied cutting configuration.

The complete understanding of the cutting process and especially resulting tools wearing requires knowledge of the thermal effects in the cutting zone. Some previous studies (see [3] for example) on the wear process have shown that the high temperature at the sliding interfaces between tool and machined material is one of the most significant factors versus wear mechanisms [4]. On the other hand it is generally admitted that total amount of mechanical energy provided during the cutting process is converted into heat. As represented in Fig. 1, heat generation occurs at two specific interfaces: the tool-workpiece and the tool-veneer interfaces that lead to the clearance and rake faces of the tool respectively. The tool-workpiece friction length l' depends on the (i) visco-elastic behaviour of the disk, (ii) left off fibres on the workpiece surface, (iii) the disk radius, (iv) the tool wear. Considering the mechanical properties of workpiece material used in this study, the ratio $l'/l \ll 1$ may be described for the MDF composite, where l denotes the tool-veneer friction length. This inequality is always verified and the tool-veneer interface can be regarded as the principal heat source during machining. The heat fluxes dissipated in the tool, the workpiece and the veneer are respectively denoted ϕ_t, ϕ_w and ϕ_c. The heat generation rate as well as the heat flux repartition depends on the tool-workpiece pair materials [5] and on the cutting parameters: the feed rate and the cutting speed.

Assessment of the average temperature in the cutting zone is the subject of numerous investigations, mainly in metal machining became nowadays the interest of woodworking area researchers. The temperature distribution near the cutting edge has been investigated experimentally and some theoretical considerations have been realised. Different techniques have been applied; Okumura [6,7] studied some configurations of cutting process, including different tool and workpiece material, as well as only the tool back face rubbing against the wood workpiece. The temperature

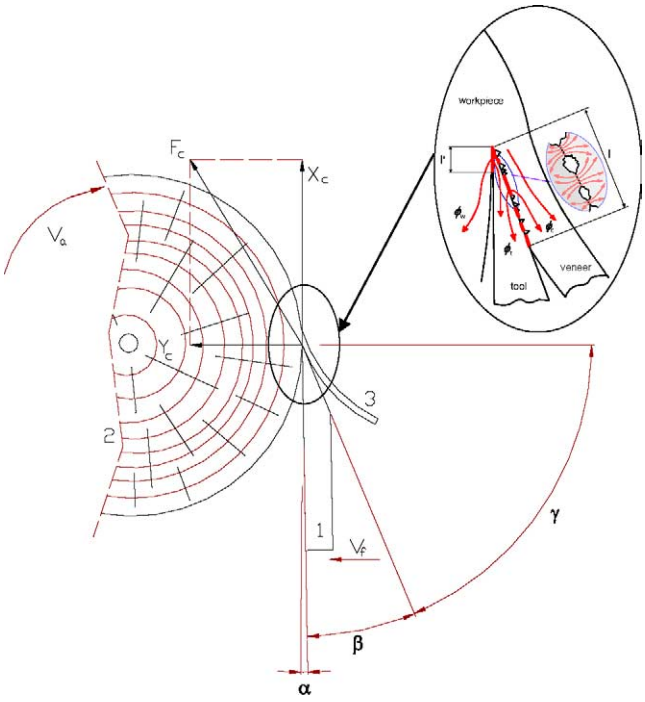

Fig. 1. Peeling process—schema of the cutting configuration: 1—knife, 2—workpiece, 3—veneer, V_a—workpiece movement (angular speed), V_f—feed, α—clearance angle, β—tool angle, γ—rake angle, F_c—cutting force. Zoom on the tool-chip-workpiece interface: ϕ_c—heat flux in the veneer, ϕ_t—heat flux in the tool, ϕ_w—heat flux in the workpiece, l—tool-veneer contact length at the rake face, l'—tool-workpiece contact at the clearance face.

measurements have been realised with an infrared detector focussed at a point of the tool face. Entire tool-chip-work system has been also investigated by thermographic camera. The infrared thermography successfully represents thermal effects in the cutting zone; unfortunately the results strongly depend on the surface emissivity that is not precisely known in practice and varies with temperature. Experiments using thermocouples located near the cutting edge have being realised, e.g., during drilling [8] or particleboard turning [9]. The measurements collected in experimental works have explicitly demonstrated high temperature gradient in the tool. The measurements at a distance from the cutting edge on the rake or clearance face do not represent real temperature value at the tool-chip interface; one can suppose that investigated temperature is much higher. In [10,11] some measurements have been realised very close to the tool tip on the side face of the tool, it does not really represent the tool-chip interface conditions. Darmawan et al. [12] in a study about performance of coated carbide tools in wood-chip cemented board machining, have built a special tool couple in order to assess the temperature at the tool-chip-workpiece interfaces from the thermal electromotive force occurring between the two cutting parts. This approach is close to natural thermocouple in metal machining with one inconvenience from machined material which is an electric insulator. This technique leads to the tool average temperature. The thermo-mechanical technique consisting in investigation of tool micro-hardness modifications after cutting experiment has been used by Hayashi et al. [13]. Another approach has been tested in [14], it consist in determination of temperature from molten regions of specially prepared vacuum deposited films within a split tool.

A less number of works concerning theoretical approaches to thermal effects at the tool-work interface during wood cutting has been found. The theoretical solution depends greatly on assumptions concerning boundary conditions and chosen part of mechanical energy converted into heat in the cutting zone. Numerical methods like boundary element, finite element or finite difference have been applied in several works [15,16]. The assumed thermal solicitations were usually arbitrarily chosen or in the manner to match experimentally measured temperatures at several locations. In the literature one can find also adaptations of analytical models developed for some metal cutting configurations. An analytical approach proposed in [17] treats a one-dimensional heat conduction problem in cylindrical coordinates. There are no presented an exact verification of agreement with experimental results. The analytical solutions confirm high temperature gradient near the cutting edge, thus the measured temperature significantly differ from the temperature at the tool veneer interface.

The direct attempts to temperature measurement at the sliding interface can represent only lower limits of temperature on the tool. In the micro-scale, the contact between tool and veneer is a part of the nominal observed area according to the surface roughness (see Fig. 1). This phenomenon causes the sliding thermal contact resistance between two solids. This thermal resistance plays a crucial role in the repartition of heat flux and temperature occurrence between the two sliding elements. Therefore, the average temperature at the interface can significantly differ from temperature on the tool. In practice the real area of tool-chip contact cannot be determined a priori. It depends on morphology of tool, roughness of the rake surface, friction coefficient, chip elastic deformation, machining parameters and varies according to the tool coating type.

Instead of the direct attempts to determine the temperature in the cutting zone, the heat flux in the tool can be estimated using an inverse approach. This inverse approach consists in estimating the heat flux from temperature measurements at one or several locations in the tool. The idea of inverse method appeared enough recently in the literature concerning metal machining [18–21]. A direct model relating the heat flux to the temperature at the sensors locations is also required. The reliability of the inverse approach depends first on the availability of the direct model to describe the real heat transfer in the tool; secondly, it depends on the measurement noise level and on the accuracy of the tool-chip contact areas measurement.

In Section 2, we present the temperature measurement device in various locations of the tool. As we show it in Section 3, the used sensors and their positioning does not make it possible to use a discrete model, of finite elements

type, as the direct model for the estimate of the heat flux spatial variation on the cutting edge of the tool versus time. We propose then, in Section 4, to use the system identification method to work out a reliable model binding the average heat flux on the heated zone according to the temperature at the sensors. As we will see it, this method requires developing a specific bench making it possible to control and measure the heat flux applied to the tool. The application is developed in Section 5. It concerns the heat flux estimation in the tool in order to evaluate the influence of CrN coating during peeling. CrN coating is deposited by PVD magnetron sputtering; its average thickness is 2 μm. Some previous studies have shown that such a coating on the tool decreases the friction coefficient at the tool-veneer interface and consequently decreases the consumed mechanical power and the tool wear [22]. Consequently, this coating leads to decrease the average temperature in the cutting zone and improves the veneer surface quality. Peeling experiments with CrN coated tool and uncoated one using the laboratory micro lathe have been realised. The machined material is a wood composite of MDF type whose density variation along the thickness gives place to a heat flux variation along the cutting edge. We use the finite elements model then to obtain a representation of this variation and we adjust the value of this variation starting from the average heat flux previously estimated. A discussion is given in section 6 in order to connect the flux consumed in the tool to the total mechanical power deduced from the efforts measurement.

2. Temperature measurement in the tool

If one seeks to reach the average heat flux on the cutting edge versus time or more precisely its spatial variation, it is obvious that uncertainty on the result of the estimate will be less if the number of sensors is large and that one carries out a great number of time sampling. Increasing the number of sensors and the sampling rate of measurements will have as a direct consequence to minimize the influence of the noise during the inversion of measurements. Moreover this estimate will be all the more reliable as the sensors will be placed as close as possible to the heated area.

In the studied cutting configuration the tool veneer contact zone length issues from the machined disk thickness, which is 14 mm. In this configuration the minimal distance between the cutting edge and the sensor can only be approximately 5 mm. It is the acceptable minimal distance so that one does not degrade the mechanical resistance of the tool because of the sensors implementation.

In this experiment micro thermistors are used, instead of thermocouples, given to their reliability and low sensitivity to vibrations during machining process. The allowed temperature measurement range, from −50 to 150 °C, and time response 200 ms are well adapted in the present configuration. Dimensions of the used thermistor are 4 mm length and 0.5 mm diameter. It must be noted that this length is of the same order of magnitude that the distance between the cutting edge and the sensor. Thereby, measurement cannot be considered as punctual and the contact between each sensor and the tool material can differ from another. It imposes consideration of the thermistor in modelling of heat conduction in the tool.

Five thermistors are fixed with a high conductive adhesive in 0.6 mm diameter holes drilled by electro discharge method. The sensors are placed symmetrically as represented in Fig. 2. It must be accented here, that their positions in the tool are assumed approximately. A current generator supplies very weak constant current equal 10 μA to each thermistor in order to avoid of self heating phenomena. The resistance of the thermistor changes according to its temperature, so the measurement of voltage V on the thermistor leads to the temperature using the following relation:

$$T(t) = \left(\frac{V}{10^{-5}}\right)^{-0.14} 602.65 - 139.35 \tag{1}$$

obtained from calibration data supplied by the manufacturer.

Acquisition of the data and parallel sensor temperature determination is realised by National Instruments Acquisition Card connected with a computer and treated by Lab VIEW software. The data acquisition system is schematically represented in Fig. 2.

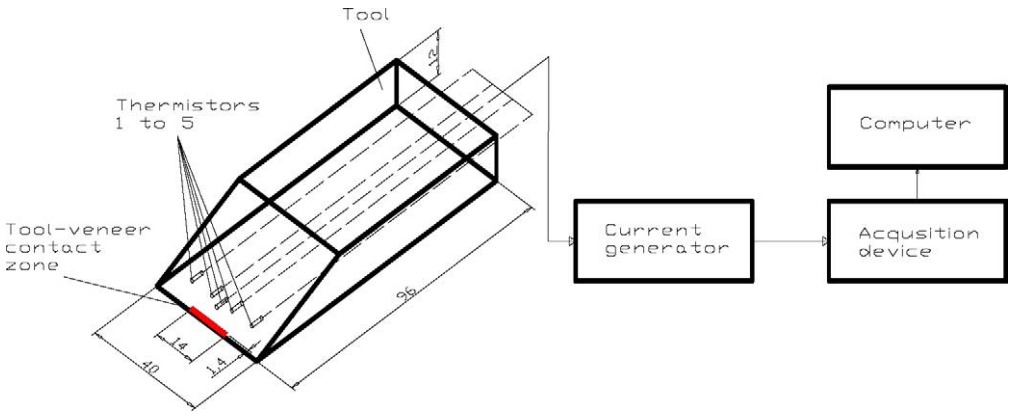

Fig. 2. Schema of the temperature measurement in the tool during cutting process.

3. Sensitivity analysis to measurement location error

Initially, we used the finite element method, applied to a spatial discretization of the tool by linear tetrahedral elements of Lagrange-quadratic type. The center of the five sensors are positioned upon the mesh that leads to the five nodes labels N_m $(m = 1, \ldots, 5)$. As we saw in the previous section, the thermal sensors used give a measurement in a bulk which one cannot reduce to a point on the mesh of the tool. In addition, the sensors location is known with much uncertainty. It is thus significant to analyze the influence of such an error on the estimate of the heat flux applied to the heated area.

The thermal conductivity and diffusivity of the knife and the knife holder are 30 $W{\cdot}m^{-1}{\cdot}K^{-1}$ and 10^{-5} $m^2{\cdot}s^{-1}$ respectively chosen approximately as for the low chromium steel [23]. The exchange coefficient, by natural convection, with the ambient is assumed to be constant and equal to 10 $W{\cdot}m^{-2}{\cdot}K^{-1}$. As verified through numerical experiments, small variations of this last parameter have no significant influence on the temperature of the sensors during the duration of machining.

A spatially uniform heat flux chosen 10 W is applied on the tool-veneer area and the temperature at each node of the mesh is calculated. A random error of zero mean and 5% standard deviation is added to the calculated value at nodes N_m. The demonstration consists in estimating the heat flux for spatial displacements of nodes N_m as: $x(N_m) = x(N_m) \pm 1$ mm, that corresponds to the sensor dimensions given in the previous section. The heat flux is estimated using the algorithm described in Appendix B. The sampling period for the estimation is $\Delta t = 1$ second and the number of future time steps is $r = 3$. The results of estimations are represented in Fig. 3.

As it is seen, the discrete model that we used is not reliable for the estimate of a uniform heat flux applied to the tool because of the nonpunctuality of measurement. Consequently, this model is even less usable for the estimate of the spatial heat flux variation on the heated area.

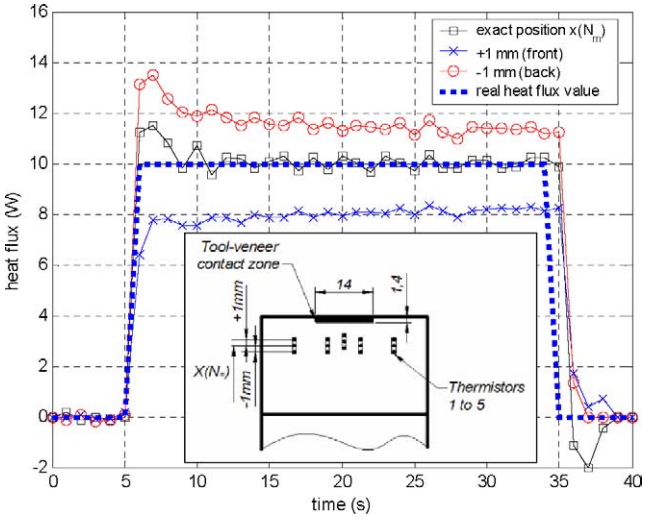

Fig. 3. Analysis of the direct discrete model sensitivity to the error of measurement position.

A more reliable model binding the average heat flux to the temperature of the sensors is obtained using the system identification method described hereafter.

4. Obtaining the direct model from the noninteger system identification

4.1. Theory

The principles of the system identification method are presented by Ljung [24]. Assuming a *linear* and *stationary* system, that is the thermal properties of the system do not vary with temperature and time, the method consists in identifying a linear relation between the heat flux $\phi(t)$ and the temperature $T_M(t)$, at each M sensor location, from measurements of these two quantities. The assumption of linearity appears correctly posed with regard to the range of temperature variation reached in the application. The most general relationship is on the following form

$$\sum_{i=L_0}^{L} \alpha_i \mathrm{D}^{n_i} T_M(t) = \sum_{i=M_0}^{M} \beta_i \mathrm{D}^{n_i} \phi(t) \tag{2}$$

In this equation, symbol D^{n_i} denotes the differentiation operator $\mathrm{d}^{n_i}/\mathrm{d}t^{n_i}$, $\{\alpha_i, \beta_i\}$ are the model parameters. The value of the bounds (L_0, L, M_0, M) in the series essentially depends on the distance between the heated surface and the sensor location and on the time range.

In the literature the differential orders n_i are integers. Nevertheless, as demonstrated by Battaglia et al. [25] in case of heat diffusion, the differentiation order in relation (2) must be

$$n_i = \frac{i}{2} \tag{3}$$

This result makes it possible to have to identify only the parameters $\{\alpha_i, \beta_i\}$ of the model, which is realized through linear minimisation. It is not any more the case when one must also identify the commensurable order of derivation (see [26] in this case). The D^{n_i} operator, when n_i have real values, is called the fractional derivative. The system identification method based on fractional calculus has been developed in the previous paper [25] and presented in Appendix C. Given to the noise measurement, it is better using the fractional integral I^{ν} $(\nu \in R)$ instead of the fractional derivative in relation (2). Given to the fundamental property: $\mathrm{D}^{-\nu} = \mathrm{I}^{\nu}$, relation (2) becomes

$$\sum_{i=L_0}^{L} \alpha_i \mathrm{I}^{n_i} T_M(t) = \sum_{i=M_0}^{N} \beta_i \mathrm{I}^{n_i} \phi(t), \quad \alpha_0 = 1 \tag{4}$$

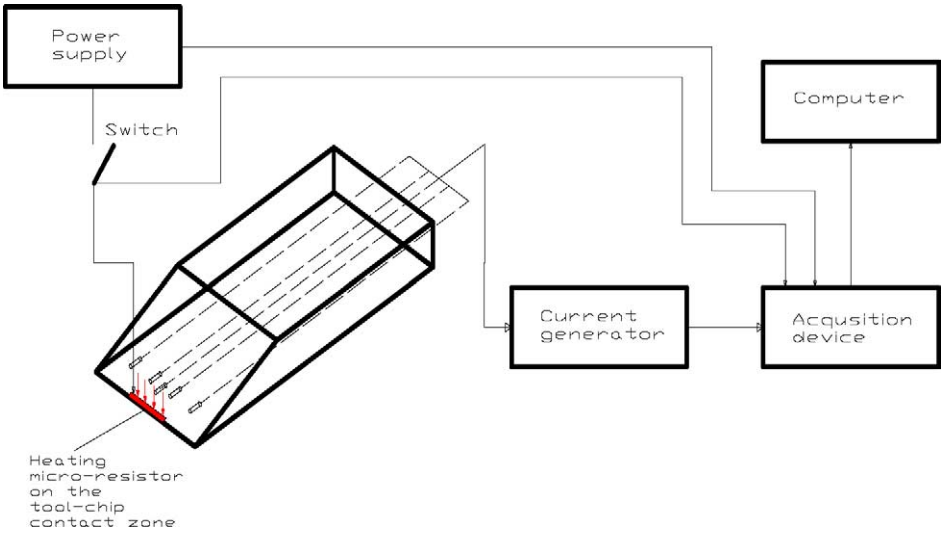

Fig. 4. Experimental apparatus for the system identification.

4.2. Experimental apparatus for the system identification

To simulate similar conditions on the tool like those occurring during machining, the micro heating device schematically represented in Fig. 4 has been developed. The heat flux is provided by a micro resistor formed as hot wire 14 mm length and 1.4 mm width. Dimensions of the micro resistor have been chosen with respect to the knife-veneer friction area encountered during the cutting process. This micro resistor has also a weak thermal inertia; less than 100 ms. One surface of the micro resistor is held in contact with the rake face of the tool, while opposite face is insulated by synthetic foam simultaneously playing the role of elastic support for the micro resistor in order to ensure an optimal tool-resistor contact. It must be noted here that the tool-veneer contact area is measured on the tool after the machining process. In order to reduce the thermal contact resistance between the micro-resistor and the tool, silver conductive grease has been introduced at the interface. The electric power provided to the micro resistor is assumed to be totally converted into heat and the heat flux from the micro resistor is supposed to be completely dissipated in the knife. This means that the heat flux in the knife is equal to the consumed electric power.

5. Application and results

5.1. Average heat flux estimation

5.1.1. Non-integer system identification

Both CrN coated and uncoated knives had to be identified because both knives were independently instrumented with thermistors, five for each according to schema in Fig. 2. Thereby, each knife constitutes a unique system with regard to the different location of the thermistors. The example of experimental data, i.e., applied heat flux and the temperatures measured in the uncoated knife are represented in

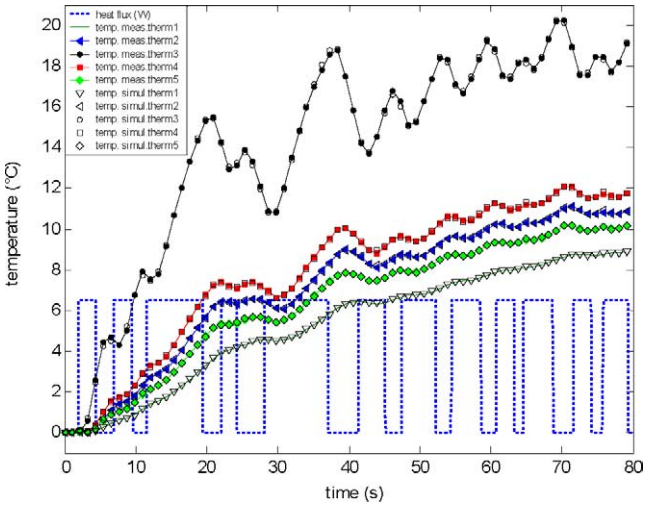

Fig. 5. Experimental data (heat flux on the tool and temperatures at the sensors) obtained during the system identification of the uncoated tool. The comparison between temperatures measured by sensors and computed from identified models (temp. meas.—measured temperature; temp. simul.—computed temperature; therm "n°"—the thermistor number).

Fig. 5. In order to accurately identify the thermal behaviour of the tool at the small and the long times the heat flux is generated in the form of different length steps. The sampling period during the identification stage was 0.02 second and duration of the experiment was 80 seconds. The numerical computing of noninteger integrals in identification algorithm imposes short sampling period in order to obtain precise results. Algorithm, described in Appendix C, was used to estimate $\{\alpha_i, \beta_i\}$ parameters of models represented in the form of relation (4) between applied heat flux and temperatures measured by thermistors. The number of parameters in the noninteger model essentially depends on the distance between the heated surface and the measurement location. It is chosen regarding the variance of the vector of residues $\mathbf{E}_K$ (see [21]). Tables 1 and 2 collect the estimated parameters

Table 1
Parameters of noninteger models identified for uncoated tool (standard deviations in parenthesis)

Sensor number (model)	Parameters								
	α_0 ($\Delta\alpha_0$)	α_1 ($\Delta\alpha_1$)	α_2 ($\Delta\alpha_2$)	α_3 ($\Delta\alpha_3$)	α_4 ($\Delta\alpha_4$)	β_0 ($\Delta\beta_0$)	β_1 ($\Delta\beta_1$)	β_2 ($\Delta\beta_2$)	β_3 ($\Delta\beta_3$)
1	1	−0.2502	0.2348	−0.0166	0.0017	−0.0148	0.0619	−0.0907	0.0476
	(0)	(1.18e-5)	(3.96e-7)	(6.15e-8)	(2.32e-10)	(7.49e-8)	(6.12e-7)	(8.61e-7)	(1.51e-7)
2	1	−0.1312	0.3827	0.0205	0.0008	−0.0453	0.2168	−0.3545	0.2071
	(0)	(7.21e-6)	(7.62e-7)	(1.31e-7)	(2.33e-10)	(3.67e-7)	(3.60e-6)	(5.94e-6)	(1.29e-6)
3	1	0.5019	0.8113	0.3230	−0.0047	−0.1458	1.0170	−2.4341	2.0624
	(0)	(1.54e-5)	(6.15e-6)	(3.11e-6)	(1.25e-9)	(5.28e-6)	(9.12e-5)	(2.56e-4)	(1.03e-4)
4	1	−0.0462	0.4338	0.0360	0.0005	−0.0490	0.2504	−0.4438	0.2796
	(0)	(4.51e-6)	(7.17e-7)	(1.04e-7)	(1.38e-10)	(2.83e-7)	(3.02e-6)	(5.43e-6)	(1.31e-6)
5	1	−0.1111	0.2749	−0.0085	0.0017	−0.0185	0.0872	−0.1423	0.0832
	(0)	(1.50e-5)	(5.70e-7)	(7.36e-8)	(1.89e-10)	(1.41e-7)	(1.31e-6)	(2.12e-6)	(4.39e-7)

Table 2
Parameters of noninteger models identified for CrN coated tool

Sensor number (model)	Parameters								
	α_0 ($\Delta\alpha_0$)	α_1 ($\Delta\alpha_1$)	α_2 ($\Delta\alpha_2$)	α_3 ($\Delta\alpha_3$)	α_4 ($\Delta\alpha_4$)	β_0 ($\Delta\beta_0$)	β_1 ($\Delta\beta_1$)	β_2 ($\Delta\beta_2$)	β_3 ($\Delta\beta_3$)
1	1	−0.0677	0.2821	−0.0034	0.0014	−0.0193	0.1068	−0.1771	0.1055
	(0)	(1.00e-5)	(0.44e-6)	(0.06e-6)	(0.01e-7)	(1.19e-7)	(1.15e-6)	(1.83e-6)	(3.94e-7)
2	1	−0.0834	0.4599	0.0522	0.0002	−0.0535	0.3169	−0.5964	0.3906
	(0)	(4.39e-6)	(7.39e-7)	(1.48e-7)	(0.01e-8)	(4.81e-7)	(5.25e-6)	(9.50e-6)	(2.41e-6)
3	1	0.1585	0.6330	0.1766	−0.0020	−0.0595	0.5044	−1.3549	1.1997
	(0)	(8.55e-6)	(2.96e-6)	(1.22e-6)	(0.01e-7)	(0.27e-5)	(4.03e-5)	(1.02e-4)	(3.78e-4)
4	1	−0.2076	0.3627	0.0098	0.0011	−0.0347	0.1836	−0.2986	0.1728
	(0)	(4.82e-6)	(5.08e-7)	(0.74e-7)	(0.01e-9)	(2.32e-7)	(2.11e-6)	(3.24e-6)	(6.73e-6)
5	1	−0.1131	0.2894	−0.0077	0.0016	−0.0166	0.0913	−0.1548	0.0936
	(0)	(1.13e-5)	(0.61e-6)	(0.06e-6)	(0.01e-8)	(1.30e-7)	(1.22e-6)	(1.95e-6)	(4.17e-7)

for uncoated and coated tool respectively. Calculated temperatures from the identified systems and previous measured heat flux are plotted in Fig. 5. A good agreement between the calculated and measured temperature was found for each model. In order to validate the identification results, another experiment must be realised. The temperatures at the sensors for a new variation of applied heat flux were computed using previously identified models. Results of computing are compared with measured temperature in Fig. 6. The excellent agreement demonstrates that identified models are accurate for any variation of the heat flux. It must be also noticed that a small number of parameters is sufficient to fit precisely the measurements.

The impulse responses for each sensor along with their confidence interval are calculated from previously identified models (see Appendix C). The same procedure was repeated for identification of CrN coated tool.

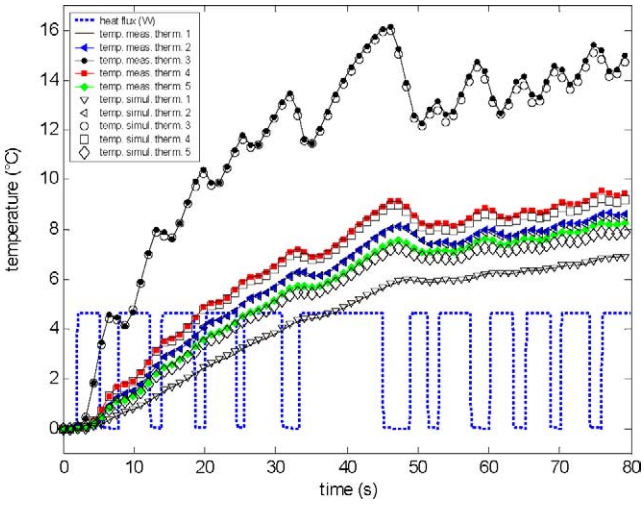

Fig. 6. Validation of the identified models (uncoated tool)—comparison between temperatures measured by sensors during second experiment and computed from identified models in the first one.

5.2. Reliability of the system identification approach

The system identification experiment is carried out by heating an approximately determined area on the rake face of the knife. Nevertheless, in practice, a part of this heat flux also comes from the tool-workpiece interface, that is from the clearance face of the tool. Even if its length l' is small with respect to the tool-veneer contact length l, it is important to know if the clearance zone significantly modifies the heat transfer in the tool and thus the temperature at the points of measurement. For that we use the finite elements model previously described and we consider three distinct geomet-

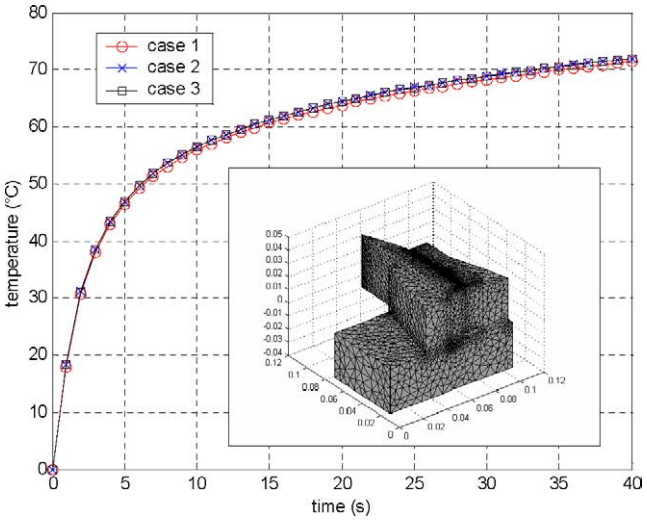

Fig. 7. Temperature evolutions at the middle sensor according to the heat flux repartition between the rake and the clearance face of the knife. The FEM geometry is represented below the graph.

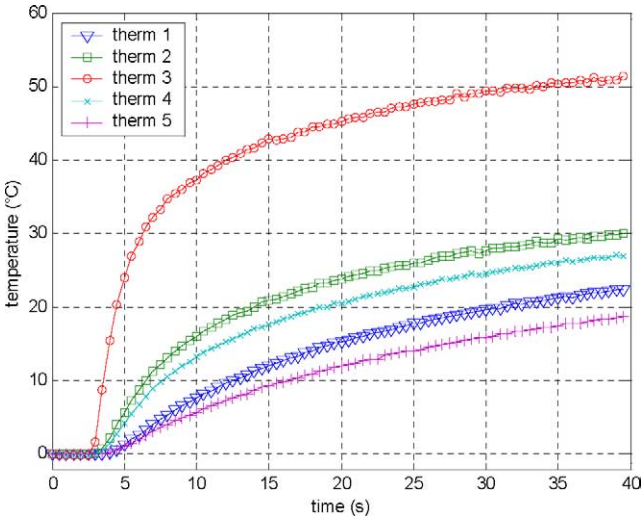

Fig. 8. Example of the temperature measured by all the thermistors in the tool during MDF peeling with uncoated tool. The cutting speed is 0.5 m·s^{-1} and the veneer thickness 0.5 mm.

rical configurations. In the first configuration, one supposes that the contact area on the clearance face is null and total heat flux is applied to the cutting face. In the second configuration, 70% of flux is applied to the cutting face and 30% on the clearance face. The height of the contact area on the clearance face is equal to 0.7 mm. In the third configuration, 50% of flux is applied to the cutting face and 50% on the clearance face. The height of the contact area on the clearance face is equal to 1.4 mm. The height of the contact area on the cutting face is equal to 1.4 mm in the three configurations. In three cases, total heat flux is equal to 10 W. We represent in Fig. 7 the temperature of sensor 3, positioned the closest to the heated zone, for the three studied cases. We note that the gap between the three curves is not significant. Thus, this enables us to conclude that a variation of the heat flux area, in a field limited by the two preceding configurations, has little influence on the temperature with the nearest sensor. It will be obviously the same for the sensors (1, 2, 4 and 5) more distant.

In other words the identified system will make it possible to estimate very precisely the heat flux applied to the tool during machining when the contact area on the clearance zone evolves from 0 to 1.4 mm.

5.3. Average heat flux estimation during the machining process

Two series of peeling process have been realised, the first with uncoated tool and the second with CrN coated. The same clearance angle $\alpha = 1°$ and tool angle $\beta = 20°$ were fixed for both knives. The principal aim of the application is the evaluation of the coatings influence on the thermal phenomena during cutting. To make this study complete the peeling process was realised at three cutting speed: 0.2, 0.5 and 1 m·s^{-1}; next at three values of veneer thickness: 0.2, 0.5, 1 mm; keeping the cutting speed at 0.5 m·s^{-1}. MDF was used as the workpiece material. The continuous peeling process has been carried out by about 50 seconds. The initial diameter of the disk was 200 mm and the final was the function of the process duration and the cutting speed. The minimal achieved final diameter was 60 mm.

The example of five temperature data measured in the tool is represented in Fig. 8; from realised measurements the average heat flux in the tool is estimated. All the temperature measurements have been carried out with the sampling period $\Delta t = 0.2$ sec. The computed previously impulse responses, were then used to estimate the heat flux in the tool using the sequential method described in Appendix A. For the estimation, the measurements have been simply resampled to $\Delta t = 1$ second by considering only one on five samples. This Δt approximately corresponds to the heat diffusion time from the rake surface to the thermistor. Fig. 9 represents the estimated heat flux during processing using two knives at three cutting speeds. Fig. 10 shows the heat flux found for different veneer thickness.

As said in the introduction the mechanical energy can be considered as completely converted into heat during cutting. The measurement of cutting force F_c allows computing the mechanical power consumed during process. In this way the comparison between the heat flux estimated in the tool and the computed mechanical power demonstrate the rate of heat evacuated by the tool from the cutting zone and its relationship with the cutting parameters. The piezoelectric system of the micro lathe permits to measure components X_c and Y_c during peeling experiments. The measurement was carried out during the process and the averages values were determined. From the resultant F_c and the cutting speed the mechanical power was obtained and the results are given in Table 3. The example of two components measurement is presented in Fig. 11.

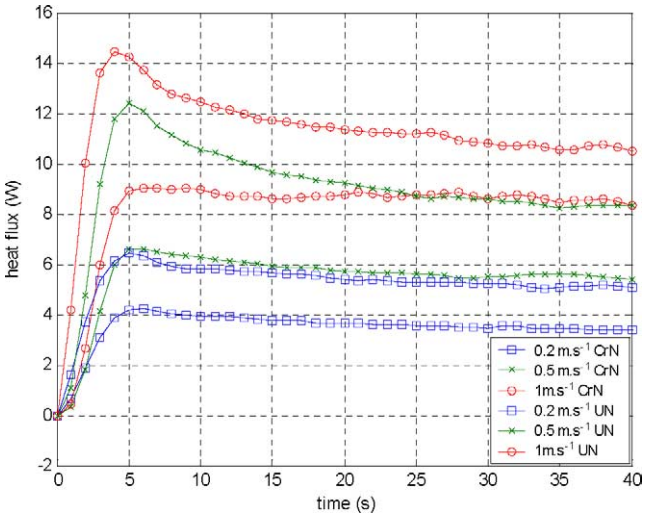

Fig. 9. Heat flux estimated during MDF peeling process at various cutting speed using CrN coated and uncoated tool.

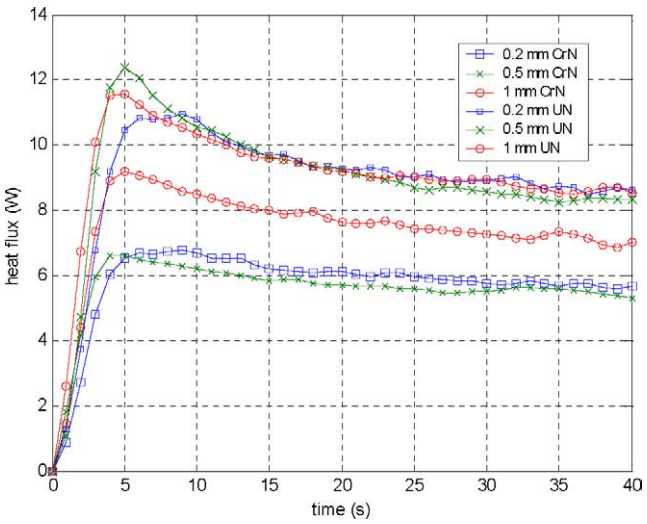

Fig. 10. Heat flux estimated during MDF peeling process with various veneer thickness using CrN coated and uncoated tool.

Table 3
Averages values of the heat flux in the knife and the mechanical power during peeling; with two knives

	Uncoated			CrN coated		
Veneer thickness [mm]	0.5			0.5		
Cutting speed [m·s^{-1}]	0.2	0.5	1	0.2	0.5	1
Approximate heat flux value [W]	5	9	11	4	5.5	8.8
Mechanical power [W]	37.6	99.4	185.6	32.3	79.8	167.2
Ratio [%]	13.3	9.0	5.9	12.4	6.9	5.3
Cutting speed [m·s^{-1}]	0.5			0.5		
Veneer thickness [mm]	0.2	0.5	1	0.2	0.5	1
Approximate heat flux value [W]	9	9	9	5.5	5.5	7.1
Mechanical power [W]	118.8	99.4	143.2	63.8	79.8	122.0
Ratio [%]	7.6	9.0	6.3	8.6	6.9	5.8

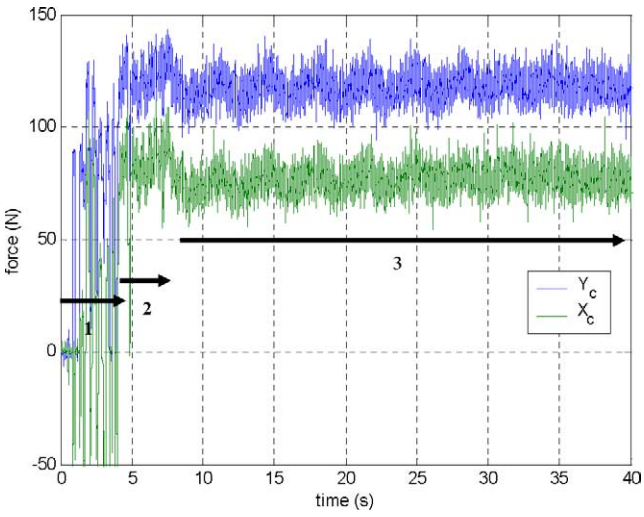

Fig. 11. Example of the cutting force measurement during machining with uncoated tool. The cutting speed is 0.5 m·s^{-1} and the veneer thickness 0.5 mm.

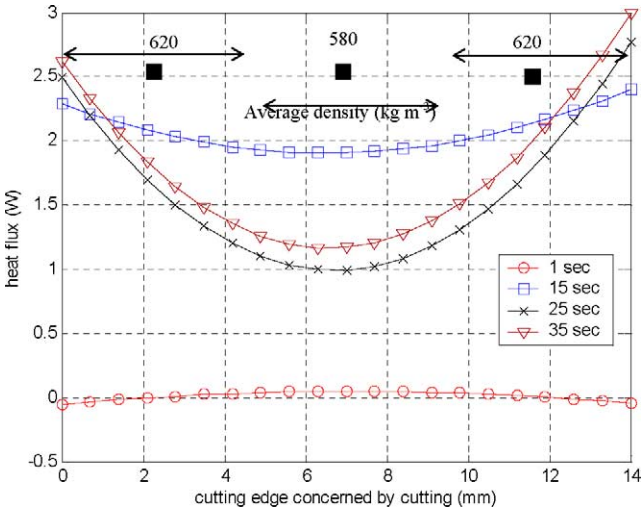

Fig. 12. Heat flux distribution along the cutting edge concerned by cutting of MDF.

5.4. Heat flux repartition on the heated surface

As we had specified, the density variation along the thickness of the MDF disk leads to a spatial variation of the heat flux on the cutting edge. We use the finite elements model to estimate this variation. The maximum number of partitions of the requested surface is equal to the number of sensors which is 5 here. Nevertheless, beyond 3, numerical experiments show that the sensitivity to the heat flux repartition becomes null because of positioning too far away from the sensors.

In Fig. 12 we plotted the interpolated profile of the heat flux on the heated area at four different moments. One highlights well that the heat flux on the two domains located in the neighbourhood of the two faces of the disk is greater than that in the center. On the other hand, this repartition becomes even more marked according to the time evolution. This phe-

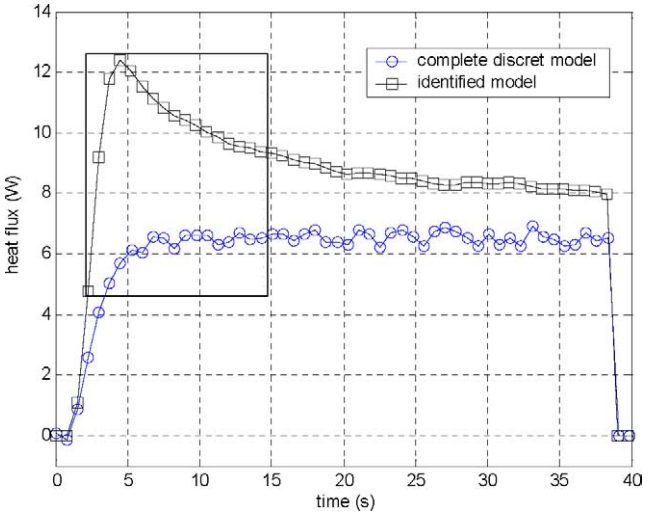

Fig. 13. Comparison between the average heat flux obtained from inversion of the identified model and the sum of three heat fluxes obtained from the complete discrete model.

nomenon corresponds well to the variation of density of the machined material, this variation coming from the compression of the two faces of the disc during its development. As an indicator this variation of density has been measured and is represented in Fig. 12. The decrease of flux in the center of the edge seems exaggerated with respect to the real phenomenon. It would thus be necessary to instrument the tool with more sensors, located closer to the edge, but as we announced that significantly increases the risks of degradations of the tool during machining. By plotting, in Fig. 13 the sum of the previous identified three fluxes versus time, one obtains a constant flux which value is rather close to that estimated it the previous section for the same cutting conditions. Nevertheless, one does not find the same dynamic as one highlighted in Fig. 13. In our opinion, that comes from the weak sensitivity already discussed previously.

6. Discussion

The experimental approach treats different configurations of the peeling process parameters in comparative intention. In this way the average heat flux in the tool was found dependent on the cutting speed. The relationship between the veneer thickness and the estimated heat flux appears not so evident.

The estimated average heat flux slightly decreases during the process. In fact, the cutting conditions are constant during one experiment; however this is an approximation regarding the variable diameter of the disk while processing. In this study, the clearance angle has been fixed as the veneer thickness does not exceed 1 mm. Nevertheless, the clearance angle should be adapted according to the disk diameter in order to keep constant contact surface at the clearance and the acting on the knife forces rapport [27]. This is not the case on the lathe used here.

The most important finding concerns the reduction of the heat flux in the knife by CrN coating. The similar results were obtained from the cutting force measurements. These measurements demonstrate higher power consumption rate during peeling with uncoated tool. The cutting force measurements are also explicative for the estimated heat flux evolution. In Fig. 11, region 1, one observes during the first 3 seconds the tool engagement and the refusal from the workpiece that involves important vibrations. Such a behaviour yields from the relatively low cutting speed (1 $m \cdot s^{-1}$ maximal) and not perfectly circular form of the work piece at the beginning of the cutting process. This phenomenon is the principal one for the slow heat flux slope reason. On the other hand, it clearly appears in Fig. 11, region 2, that the mechanical power slightly increases. One observes the same evolution on the heat flux in the tool at the beginning of machining. Furthermore, given to the heat flux magnitude in region 2, it seems that the heat flux reparation in the tool, the veneer and the workpiece evolves in this region and becomes constant after, region 3.

The ratio between the estimated heat flux in the tool and the consumed mechanical power reveals the knife in the studied process is not the principal way of heat evacuation from the cutting zone. The heat flux in the knife is less than 15% of the mechanical energy. The relationship between the cutting parameters and the found ratio can be driven. One observes the ratio decrease versus the cutting speed and the veneer thickness increase.

Considering the length of the working cutting edge and the composition of the machined material in the present application, attention must be paid to the spatial distribution of the heat flux in the tool. The heat flux variation in the tool follows overall the density variation of the material whatever the type of coating. This variation thus generates a spatial repartition of the temperature on the cutting face which leads to a nonhomogeneous wear of the tool.

7. Conclusion

This study highlighted the influence of a CrN coating and the various cutting parameters one the average heat flux in a cutting tool during wood peeling process. This average heat flux is estimated from temperature measurements in the tool using microthermistors embedded at several locations along the cutting edge. The inherent difficulty in this inverse heat conduction problem comes from the type of used sensor. Indeed, measurement is not punctual and the size of the sensors leads to necessity to take into account their dynamics in the heat transfer model in the tool. Thus, a classical model of finite elements type making it possible to consider the variation space–time of flux on the requested zone proves to be unsuited. The model binding average flux to the temperature at the measurement locations is obtained in the system identification sense. For that, it was necessary to work out a specific experimental bench making it possible to control

and measure the heat flux applied to the tool. The parameters of the model based on the noninteger order integration operator are identified starting from measurements of heat flux and temperature of the sensors. This model is then used in an algorithm of inversion to estimate the average heat flux versus the time during the machining process.

The results obtained clearly highlight the role of the CrN coating on the tool, in particular when one jointly analyzes measurements of efforts and thus the total power consumed during the cut. The space variability of heat flux along the heated zone is highlighted by the use of the finite elements model and the results attest variation of the work material density along the disk thickness. Nevertheless, as we showed, these results must be analyzed with many precautions being given the low sensitivity obtained from the sensor localization far away with respect to the cutting edge.

Appendix A. Constant function specification method

The objective is to estimate the heat flux in the tool $\hat{\phi}(t)$ at the time t from realised temperature measurements $Y_M(t)$ at the time t, point M and previous instants with a sampling period Δt. The convolution theorem leads expressing the temperature at a sensor located at point M according to the heat flux as

$$T_M(K\Delta t) = \sum_{l=0}^{K} h_M\big((K-l)\Delta t\big)\phi(l\Delta t) \tag{A.1}$$

$h_M(l\Delta t)$ is the impulse response at time $t = l\Delta t$ and point M, calculated from the model of heat transfer in the tool by replacing $\phi(t)$ with the Dirac function $\delta(t)$. In order to solve the inverse heat conduction problem in the tool (estimation of the boundary condition), the constant function specification method is applied. Detailed description of this method is presented by Beck [28]. The method assumes a constant estimated heat flux from instant t to $t + r\Delta t$, where r denotes the number of future time steps. The estimated heat flux $\hat{\phi}(K\Delta t)$ at time $t = K\Delta t$ is then given by

$$\hat{\phi}(K\Delta t) = \left\{ \sum_{j=1}^{r} \sum_{M=1}^{J} \Big(Y_M\big(\big((K+j-1)\Delta t\big)\big) - \widetilde{T}_M\big((K+j-1)\Delta t\big)\Big)\, \mathrm{d}h_{j,M} \right\} \times \left[\sum_{j=1}^{r} \sum_{M=1}^{J} \mathrm{d}h_{j,M}^2 \right]^{-1} \tag{A.2}$$

where J is the number of sensors and $Y_M(K\Delta t)$ is the temperature measured from the sensor M at time $t = K\Delta t$ with

$$\mathrm{d}h_{j,M} = \sum_{i=1}^{j} h_M((i\Delta t)) \tag{A.3}$$

and

$$\widetilde{T}_M\big(\big((K+i-1)\Delta t\big)\big) = \sum_{l=1}^{K-1} h_M\big((K+i-l)\Delta t\big)\hat{\phi}(l\Delta t) + T_M(0) \tag{A.4}$$

$T_M(0)$ is the initial temperature from the sensor M.

The sampling period Δt for the estimation is chosen close to the diffusion time from the heated surface to the largest distance between the sensors and the tool-veneer interface according to $\Delta t \approx L^2/\alpha$, where L is the distance and α the thermal diffusivity of the tool material.

Appendix B. Solution of the inverse heat conduction problem using the complete discrete model

Using the finite element method the direct model is written in the following matrix form

$$\mathbf{C}_p \frac{\mathrm{d}\mathbf{T}}{\mathrm{d}t} = \mathbf{A}\mathbf{T}(t) + \mathbf{B}\mathbf{U}(t) \tag{B.1}$$

$$\mathbf{Y}(t) = \mathbf{C}\mathbf{T}(t) \tag{B.2}$$

In these relations $\mathbf{T}(t)$ is the vector that collects the temperatures on the N nodes of the mesh, $\mathbf{C}_p(\mathrm{N}\times\mathrm{N})$ is the matrix of the heat capacity, $\mathbf{A}(\mathrm{N}\times\mathrm{N})$ is the state (or evolution) matrix, $\mathbf{B}(\mathrm{N}\times\mathrm{P})$ is the input (or control) matrix and $\mathbf{C}(\mathrm{M}\times\mathrm{N})$ is the output (or observation) matrix which precise the measurement positions on the M mesh nodes. Finally $\mathbf{U}(t)(\mathrm{P}\times 1)$ is the input vector.

The implicit discretisation of relations (B.1) and (B.2) lead to

$$\mathbf{T}^{(n)} = \mathbf{D}\mathbf{T}^{(n-1)} + \mathbf{F}\mathbf{U}^{(n)} \tag{B.3}$$

$$\mathbf{Y}^{(n)} = \mathbf{C}\mathbf{T}^{(n)} \tag{B.4}$$

with

$$\mathbf{D} = \big(\mathbf{I}_n - \Delta t\mathbf{C}_p^{-1}\mathbf{A}\big)^{-1}, \qquad \mathbf{F} = \Delta t\mathbf{D}\mathbf{C}_p^{-1}\mathbf{B} \tag{B.5}$$

Replacing (n) with $(n+1)$ in relations (B.3), (B.4) gives

$$\mathbf{Y}^{(n+1)} = \mathbf{C}\mathbf{D}\mathbf{T}^{(n)} + \mathbf{C}\mathbf{F}\mathbf{U}^{(n+1)} \tag{B.6}$$

Substituting $\mathbf{T}^{(n)}$ by its expression from relation (B.3) one obtains

$$\mathbf{Y}^{(n+1)} = \mathbf{C}\mathbf{D}^2\mathbf{T}^{(n-1)} + \mathbf{C}\mathbf{D}\mathbf{F}\mathbf{U}^{(n+1)} + \mathbf{C}\mathbf{F}\mathbf{U}^{(n)} \tag{B.7}$$

Repeating this $(n+r)$ times with r future time steps one finds

$$\begin{aligned} &\mathbf{Y}^{(n)} = \mathbf{C}\mathbf{D}\mathbf{T}^{(n-1)} + \mathbf{C}\mathbf{F}\mathbf{U}^{(n)} \\ &\mathbf{Y}^{(n+1)} = \mathbf{C}\mathbf{D}^2\mathbf{T}^{(n-1)} + \mathbf{C}\mathbf{D}\mathbf{F}\mathbf{U}^{(n+1)} + \mathbf{C}\mathbf{F}\mathbf{U}^{(n)} \\ &\quad\vdots \\ &\mathbf{Y}^{(n+r)} = \mathbf{C}\mathbf{D}^{n+r+1}\mathbf{T}^{(n-1)} + \mathbf{C}\mathbf{D}^{r-1}\mathbf{F}\mathbf{U}^{(n+r)} \\ &\quad + \mathbf{C}\mathbf{D}^{r-2}\mathbf{F}\mathbf{U}^{(n+r-1)} + \cdots + \mathbf{C}\mathbf{F}\mathbf{U}^{(n)} \end{aligned} \tag{B.8}$$

This can be written in the matrix form as

$$\mathbf{Y} = \widetilde{\mathbf{T}} + \mathbf{X}\mathbf{U} \tag{B.9}$$

with

$$\mathbf{Y}=\begin{bmatrix}\mathbf{Y}^{(n)}\\ \mathbf{Y}^{(n+1)}\\ \vdots\\ \mathbf{Y}^{(n+r)}\end{bmatrix},\qquad \widetilde{\mathbf{T}}=\begin{bmatrix}\mathbf{CDT}^{(n-1)}\\ \mathbf{CD}^{2}\mathbf{T}^{(n-1)}\\ \vdots\\ \mathbf{CD}^{n+r+1}\mathbf{T}^{(n-1)}\end{bmatrix}\quad\text{and}$$

$$\mathbf{X}=\begin{bmatrix}\mathbf{CF}\\ \mathbf{CDF}+\mathbf{CF}\\ \vdots\\ \mathbf{CD}^{r-1}\mathbf{F}+\mathbf{CD}^{r-2}\mathbf{F}+\cdots+\mathbf{CF}\end{bmatrix} \tag{B.10}$$

Finally, considering $\mathbf{U}^{(n)}=\mathbf{U}^{(n+1)}=\cdots=\mathbf{U}^{(n+r)}$ the estimation of $\mathbf{U}^{(n)}$ (heat flux) in the least square sense is

$$\widehat{\mathbf{U}}^{(n)}=\left(\mathbf{X}^{\mathrm{T}}\mathbf{X}\right)^{-1}\mathbf{X}^{\mathrm{T}}\left(\mathbf{Y}-\widetilde{\mathbf{T}}\right) \tag{B.11}$$

Appendix C. System identification method

The noninteger model expressing the temperature $T_M(t)$ at the sensor M according to the heat flux $\phi(t)$ in the tool is

$$\sum_{i=L_0}^{L}\alpha_i \mathrm{I}^{n_i}T_M(t)=\sum_{i=M_0}^{M}\beta_i \mathrm{I}^{n_i}\phi(t),\quad n_i=\frac{i}{2},\ \alpha_0=1 \tag{C.1}$$

Benefiting from the equality $\mathrm{I}^{\nu}f(t)=\mathrm{D}^{-\nu}f(t)$, $\nu\in\Re$, the numerical approximation of the fractional derivative of function $f(t)$ given by Grünwald is used to compute noninteger integrals

$$\mathrm{D}^{\nu}f(t)=\frac{1}{\Delta t^{\nu}}\sum_{k=0}^{K}(-1)^k\binom{\nu}{k}f\big((K-k)\Delta t\big) \tag{C.2}$$

where Δt is the sampling period, $\nu\in\Re$ the differentiation order and

$$\binom{\nu}{k}=\frac{\nu(\nu-1)\cdots(\nu-k+1)}{k!}$$

Let us consider temperature measurement $Y_M(t)$ by the sensor M at time t, with $e_M(t)$ denoting the measurement error as

$$Y_M(t)=T_M(t)+e_M(t) \tag{C.3}$$

By replacing $T_M(t)$ in relation (C.1) from its expression in (C.3) one finds

$$\mathrm{I}^{L_0/2}Y_M(t)=\sum_{i=M_0}^{M}\beta_i \mathrm{I}^{n_i}\phi(t)-\sum_{i=L_0+1}^{L}\alpha_i \mathrm{I}^{n_i}Y_M(t)+\varepsilon_M(t) \tag{C.4}$$

The residue $\varepsilon_M(t)$ is expressed according to the measurement error as

$$\varepsilon_M(t)=\sum_{i=L_0}^{L}\alpha_i \mathrm{I}^{n_i}e_M(t) \tag{C.5}$$

The relation (C.4) is represented as the linear regression

$$\mathrm{I}^{L_0/2}Y_M(t)=\mathbf{H}_M(t)\boldsymbol{\theta}_M+\varepsilon_M(t) \tag{C.6}$$

The regression matrix is

$$\mathbf{H}_M(t)=\big[-\mathrm{I}^{(L_0+1)/2}Y_M(t)\quad\ldots\quad-\mathrm{I}^{L/2}Y_M(t)\mathrm{I}^{M_0/2}\phi(t)\quad\ldots\quad\mathrm{I}^{M/2}\phi(t)\big] \tag{C.7}$$

and the vector of unknown parameters is

$$\boldsymbol{\theta}_M=\big[\alpha_1\quad\ldots\quad\alpha_{N+1}\beta_0\quad\ldots\quad\beta_N\big]^{\mathrm{T}} \tag{C.8}$$

Performing $(K+1)$ successive measurements with constant sampling period Δt, relation (C.6) becomes

$$\mathrm{I}^{L_0/2}\mathbf{Y}_K=\mathbf{H}_K\boldsymbol{\theta}_M+\mathbf{E}_K \tag{C.9}$$

where

$$\mathbf{H}_K=\begin{bmatrix}\mathbf{H}_M(t)\\ \mathbf{H}_M(t+\Delta t)\\ \vdots\\ \mathbf{H}_M(t+K\Delta t)\end{bmatrix}\quad\text{and}\quad\mathbf{E}_K=\begin{bmatrix}\varepsilon_M(t)\\ \varepsilon_M(t+\Delta t)\\ \vdots\\ \varepsilon_M(t+K\Delta t)\end{bmatrix} \tag{C.10}$$

Because the model is identified from huge quantity of data (the number K is large), the recursive least square method is applied as the parameters estimation algorithm, where the vector of parameters at instant t is estimated from parameters estimated previously at instant $(t-1)$ according to

$$\hat{\boldsymbol{\theta}}_M(t)=\hat{\boldsymbol{\theta}}_M(t-1)+\mathbf{L}(t)\big[\mathrm{I}^{L_0/2}y(t)-\mathbf{H}_M(t)\hat{\boldsymbol{\theta}}_M(t-1)\big] \tag{C.11}$$

with

$$\mathbf{L}(t)=\frac{\mathbf{P}(t-1)\mathbf{H}_M^{\mathrm{T}}(t)}{\lambda(t)+\mathbf{H}_M(t)\mathbf{P}(t-1)\mathbf{H}_M^{\mathrm{T}}(t)} \tag{C.12}$$

$$\mathbf{P}(t)=\mathbf{P}(t-1)-\frac{\mathbf{P}(t-1)\mathbf{H}_M^{\mathrm{T}}(t)\mathbf{H}_M(t)\mathbf{P}(t-1)}{\lambda(t)+\mathbf{H}_M(t)\mathbf{P}(t-1)\mathbf{H}_M^{\mathrm{T}}(t)} \tag{C.13}$$

where the initial values are: $\hat{\boldsymbol{\theta}}_M(0)=\mathbf{0}_D$ and $\mathbf{P}(0)=10^6\mathbf{I}_D$, with $\mathbf{0}_D$ and $\mathbf{I}_D$ are zeros vector and ones matrix respectively with dimension $D=2N$.

The confidence domain of the identified parameters yields from the covariance matrix, given by

$$\mathbf{cov}\big(\hat{\boldsymbol{\theta}}_M\big)=\mathbf{P}(t_f)\frac{\sigma_{\mathrm{I}^{L_0/2}Y}}{2} \tag{C.14}$$

in the recursive least square method, where t_f denotes the final instant of estimation and

$$\sigma_Y\approx\frac{\mathbf{E}_K\mathbf{E}_K^{\mathrm{T}}}{K} \tag{C.15}$$

Computing of the impulse response. When $\phi(t)=\delta(t)$ is the Dirac function and its noninteger integral is

$$\mathrm{I}^{\nu}\delta(t)=\frac{t^{\nu-1}}{\Gamma(\nu)},\quad\text{with }\Gamma(\nu)=\int_0^{\infty}u^{\nu-1}\exp(-u)\,\mathrm{d}u \tag{C.16}$$

From (C.1), the impulse response $h(t)$ is obtained by solution of

$$h(t) = \sum_{i=0}^{N} \beta_i \frac{t^{\nu-1}}{\Gamma(\nu)} - \sum_{i=1}^{N+1} \alpha_i \mathrm{I}^{n_i} h(t) \tag{C.17}$$

Expression (C.17) permits to relate the incertitude on the impulse response directly to the confidence domain of estimated parameters α_i and β_i in the form

$$\begin{aligned} \Delta h(t) = {} & \sum_{i=0}^{N} \Delta\beta_i \mathrm{I}^{n_i} \frac{t^{i/2-1}}{\Gamma(i/2)} - \sum_{i=0}^{N+1} \Delta\alpha_i \mathrm{I}^{n_i} h(t) \\ & - \sum_{i=0}^{N+1} (\alpha_i + \Delta\alpha_i) \mathrm{I}^{n_i} \Delta h(t) \\ \alpha_0 = 1, \quad & \Delta\alpha_0 = 0 \end{aligned} \tag{C.18}$$

References

[1] J. Sheikh-Ahmad, T. Morita, Tool coatings for wood machining, in: Proceedings of 15th International Wood Machining Seminar, Loyola Marymount, USA, 2001.

[2] J.C. Butaud, C. Deces-Petit, R. Marchal, An experimental device for the study of wood cutting mechanisms: the microlathe, in: Poster Session Proceedings of the 12th International Wood Machining Seminar, Kyoto, Japan, 1995, pp. 479–485.

[3] B. Porankiewicz, Simulation of high temperature corrosion of components of cemented carbide cutting egde in contact with particle board, in: Proceedings of the 13th International Wood Machining Seminar, Vancouver, Canada, 1997, pp. 779–790.

[4] J. Sheikh-Ahmad, J.A. Bailey, High temperature wear of cemented tungsten carbide tools while machining particleboard and fiberboard, J. Wood Sci. 45 (1999) 445–455.

[5] W. Grzesik, The role of coatings in controlling the cutting process when turning with coated indexable inserts, J. Materials Processing Technol. 79 (1998) 133–143.

[6] S. Okumura, H. Sugihara, Temperature of sawtooth cusp in rubbing of the back face with wood, Bull. Kyoto Univ. Forests 53 (1981).

[7] S. Okumura, S. Nanba, M. Noguchi, Thermographic temperature measurement of tool-veneer-work system in slow-speed wood cutting, in: Proceedings of the 11th International Wood Machining Seminar, Honne, Norway, 1993, pp. 41–55.

[8] S. Okumura, H. Kuratsu, H. Sugihara, Tool temperature in machine boring of wood, Mokuzai Gakkaishi 33 (1987) 274–280.

[9] J.Y. Sheikh-Ahmad, W.M. McKenzie, Measurement of tool wear and dulling in the machining of particleboard, in: Proceedings of the 13th International Wood Machining Seminar, Vancouver, Canada, 1997, pp. 659–669.

[10] S. Okumura, T. Okuda, H. Sugihara, Temperature distribution on the side face of a saw tooth in interrupted cutting I, orthogonal cutting, Mokuzai Gakkaishi 29 (1983) 123–130.

[11] S. Okumura, H. Sugihara, T. Okuda, Temperature distribution on the side face of a saw tooth in interrupted cutting II, grooving, Mokuzai Gakkaishi 29 (1983) 131–138.

[12] W. Darmawan, Ch. Tanaka, H. Usuki, T. Othani, Performance of coated carbide tools in turning wood-based materials: Effect of cutting speeds and coating materials on the wear characteristics of coated carbide tools in turning wood-veneer cement board, J. Wood Sci. 47 (2001) 342–349.

[13] K. Hayashi, M. Oono, I. Masaaki, Estimation of tool temperature in the neighbourhood of the cutting edge in peripheral milling of wood, Mokuzai Gakkaishi 32 (1986) 603–607.

[14] S. Tsutsumi, T. Kato, K. Hayashi, Visualization of temperature distribution near the cutting edge by means of a vacuum deposition of thermoscopic film on matching surface of a split tool, Mokuzai Gakkaishi 35 (1989) 382–384.

[15] E. Csanády, Heat transfer and thermal loading in wood cutting tools, in: Proceedings of the 11th International Wood Machining Seminar, Honne, Norway, 1993, pp. 486–494.

[16] S. Okumura, A numerical analysis of tool edge temperature in rubbing against wood, in: Proceedings of the 12th International Wood Machining Seminar, Kyoto, Japan, 1995, pp. 529–537.

[17] S. Okumura, A theoretical approach to the cutting edge temperature in interrupted cutting of wood, Mem. College Agriculture, Kyoto University 127 (1985) 29–36.

[18] M.P. Lipman, B.E. Nevis, G.E. Kane, A remote sensor method for determining average tool-veneer interface temperatures in metal cutting, ASME J. Engrg. Indust. 89 (2) (1967) 333–338.

[19] D.A. Stephenson, An inverse method for investigating deformation zone temperatures in metal cutting, J. Engrg. Indust. 113 (1991) 129–136.

[20] J.-L. Battaglia, J.-C. Batsale, Estimation of heat flux and temperature in a tool during turning, Inverse Problems Engrg. 8 (2000) 435–456.

[21] J.-L. Battaglia, L. Le Lay, L.J.-Ch. Batsale, A. Oustaloup, O. Cois, Utilisation de modèles d'identification non entiers pour la résolution de problèmes inverses en conduction, Internat. J. Thermal Sci. 39 (2000) 374–389.

[22] C. Nouveau, M.-A. Djouadi, R. Marchal, M. Lambertin, Applications of hard coatings (Cr_xN_y) obtained by PVD methods in wood machining, Mécanique & Industries 3 (2002) 333–342.

[23] F.P. Incropera, D.P. DeWitt, Introduction to Heat Transfer, Wiley, New York, 1996.

[24] L. Ljung, System Identification: Theory for the User, Prentice-Hall, England Cliffs, NJ, 1987.

[25] J.-L. Battaglia, L. Puigsegur, A. Kusiak, Représentation non entière du transfert de chaleur par diffusion. Utilité pour la caractérisation et le contrôle non destructif thermique, Internat. J. Thermal Sci. 75 (4) (2003) 350–370.

[26] J.-L. Battaglia, O. Cois, L. Puigsegur, A. Oustaloup, Solving an inverse heat conduction problem using a non-integer identified model, Internat. J. Heat Mass Transfer 44 (2001) 2671–2680.

[27] CTB, Technologie du Déroulage, Cahier du Centre Technique du Bois, vol. 115, Paris, France, 1979.

[28] J. Beck, B. Blackwell, St.C.R. Clair, Inverse Heat Conduction, Wiley–Interscience, New York, 1985.